

Search for effects beyond the Born approximation in polarization transfer observables in $\vec{e}p$ elastic scattering

M. Meziane,^{1,*} E. J. Brash,^{2,3} R. Gilman,^{4,3} M. K. Jones,³ W. Luo,⁵ L. Pentchev,¹ C. F. Perdrisat,¹ A. J. R. Puckett,^{6,7} V. Punjabi,⁸ F. R. Wesselmann,⁸ A. Ahmidouch,⁹ I. Albayrak,¹⁰ K. A. Aniol,¹¹ J. Arrington,¹² A. Asaturyan,¹³ O. Ates,¹⁰ H. Baghdasaryan,¹⁴ F. Benmokhtar,¹⁵ W. Bertozzi,⁶ L. Bimbot,¹⁶ P. Bosted,³ W. Boeglin,¹⁷ C. Butuceanu,¹⁸ P. Carter,² S. Chernenko,¹⁹ E. Christy,¹⁰ M. Commisso,¹⁴ J. C. Cornejo,¹¹ S. Covrig,³ S. Danagoulian,⁹ A. Daniel,²⁰ A. Davidenko,²¹ D. Day,¹⁴ S. Dhamija,¹⁷ D. Dutta,²² R. Ent,³ S. Frullani,²³ H. Fenker,³ E. Frlez,¹⁴ F. Garibaldi,²³ D. Gaskell,³ S. Gilad,⁶ Y. Goncharenko,²¹ K. Hafidi,¹² D. Hamilton,²⁴ D. W. Higinbotham,³ W. Hinton,⁸ T. Horn,³ B. Hu,⁵ J. Huang,⁶ G. M. Huber,¹⁸ E. Jensen,² H. Kang,²⁵ C. Keppel,¹⁰ M. Khandaker,⁸ P. King,²⁰ D. Kirillov,¹⁹ M. Kohl,¹⁰ V. Kravtsov,²¹ G. Kumbartzki,⁴ Y. Li,¹⁰ V. Mamyan,¹⁴ D. J. Margaziotis,¹¹ P. Markowitz,¹⁷ A. Marsh,² Y. Matulenko,^{21,†} J. Maxwell,¹⁴ G. Mbianda,²⁶ D. Meekins,³ Y. Melnik,²¹ J. Miller,²⁷ A. Mkrtchyan,¹³ H. Mkrtchyan,¹³ B. Moffit,⁶ O. Moreno,¹¹ J. Mulholland,¹⁴ A. Narayan,²² Nuruzzaman,²² S. Nedev,²⁸ E. Piasetzky,²⁹ W. Pierce,² N. M. Piskunov,¹⁹ Y. Prok,² R. D. Ransome,⁴ D. S. Razin,¹⁹ P. E. Reimer,¹² J. Reinhold,¹⁷ O. Rondon,¹⁴ M. Shabestari,¹⁴ A. Shahinyan,¹³ K. Shesternanov,^{21,†} S. Širca,³⁰ I. Sitnik,^{19,†} L. Smykov,^{19,†} G. Smith,³ L. Solovyev,²¹ P. Solvignon,¹² R. Subedi,¹⁴ R. Suleiman,³ E. Tomasi-Gustafsson,^{31,16} A. Vasiliev,²¹ M. Vanderhaeghen,³² M. Veilleux,² B. B. Wojtsekhowski,³ S. Wood,³ Z. Ye,¹⁰ Y. Zanevsky,¹⁹ X. Zhang,⁵ Y. Zhang,⁵ X. Zheng,¹⁴ and L. Zhu¹⁰

¹The College of William and Mary, Williamsburg, Virginia 23187, USA

²Christopher Newport University, Newport News, Virginia 23606, USA

³Thomas Jefferson National Accelerator Facility, Newport News, Virginia 23606, USA

⁴Rutgers, The State University of New Jersey, Piscataway, New Jersey 08855, USA

⁵Lanzhou University, 222 Tianshui Street S., Lanzhou 730000, Gansu, People's Republic of China

⁶Massachusetts Institute of Technology, Cambridge, Massachusetts 02139, USA

⁷Los Alamos National Laboratory, Los Alamos, New Mexico 87545, USA

⁸Norfolk State University, Norfolk, Virginia 23504, USA

⁹North Carolina A&T state University, Greensboro, North Carolina 27411, USA

¹⁰Hampton University, Hampton, Virginia 23668, USA

¹¹California State University, Los Angeles, Los Angeles, California 90032, USA

¹²Argonne National Laboratory, Argonne, Illinois 60439, USA

¹³Yerevan Physics Institute, Yerevan 375036, Armenia

¹⁴University of Virginia, Charlottesville, Virginia 22904, USA

¹⁵Carnegie Mellon University, Pittsburgh, PA 15213, USA

¹⁶Institut de Physique Nucléaire, CNRS, IN2P3 and Université Paris Sud, Orsay Cedex, France

¹⁷Florida International University, Miami, Florida 33199, USA

¹⁸University of Regina, Regina, SK S4S 0A2, Canada

¹⁹JINR-LHE, Dubna, Moscow Region, Russia 141980

²⁰Ohio University, Athens, Ohio 45701, USA

²¹IHEP, Protvino, Moscow Region, Russia 142284

²²Mississippi State University, Starkeville, Mississippi 39762, USA

²³INFN, Sezione Sanità and Istituto Superiore di Sanità, 00161 Rome, Italy

²⁴University of Glasgow, Glasgow G12 8QQ, Scotland, United Kingdom

²⁵Seoul National University, Seoul 151-742, South Korea

²⁶University of Witwatersrand, Johannesburg, South Africa

²⁷University of Maryland, College Park, Maryland 20742, USA

²⁸University of Chemical Technology and Metallurgy, Sofia, Bulgaria

²⁹University of Tel Aviv, Tel Aviv, Israel

³⁰Jozef Stefan Institute, 3000 SI-1001 Ljubljana, Slovenia

³¹CEA Saclay, F-91191 Gif-sur-Yvette, France

³²Institut für Kernphysik, Johannes Gutenberg-Universität, D-55099 Mainz, Germany

(Dated: May 22, 2018)

Intensive theoretical and experimental efforts over the past decade have aimed at explaining the discrepancy between data for the proton electric to magnetic form factor ratio, G_E/G_M , obtained separately from cross section and polarization transfer measurements. One possible explanation for this difference is a two-photon-exchange (TPEX) contribution. In an effort to search for effects beyond the one-photon-exchange or Born approximation, we report measurements of polarization transfer observables in the elastic $H(\vec{e}, e'\vec{p})$ reaction for three different beam energies at a fixed squared momentum transfer $Q^2 = 2.5 \text{ GeV}^2$, spanning a wide range of the virtual photon polarization parameter, ϵ . From these measured polarization observables, we have obtained separately the

ratio R , which equals $\mu_p G_E/G_M$ in the Born approximation, and the longitudinal polarization transfer component P_ℓ , with statistical and systematic uncertainties of $\Delta R \approx \pm 0.01(\text{stat}) \pm 0.013(\text{syst})$ and $\Delta P_\ell/P_\ell^{\text{Born}} \approx \pm 0.006(\text{stat}) \pm 0.01(\text{syst})$. The ratio R is found to be independent of ϵ at the 1.5% level, while the ϵ dependence of P_ℓ shows an enhancement of $(2.3 \pm 0.6)\%$ relative to the Born approximation at large ϵ .

After decades of experimental and theoretical efforts, the internal structure of the nucleon remains one of the defining problems of nuclear physics. Based on the generally accepted notion that the electromagnetic interaction is well understood from a theoretical point of view, elastic electron-nucleon scattering has served as a powerful tool to measure fundamental observables: the electromagnetic form factors. There are two experimental methods for extracting the ratio of the electric to magnetic form factors of the proton, G_E/G_M , from electron-proton elastic scattering. In the Rosenbluth separation technique [1], G_E^2 and G_M^2 are determined from the angular dependence of the reduced cross section σ_r at constant Q^2 . Polarization experiments determine G_E/G_M by using a polarized electron beam with either a polarized proton target, or a measurement of the transferred polarization to the scattered proton. At values of the squared-momentum-transfer, $Q^2 \leq 1 \text{ GeV}^2$, data from the Rosenbluth and polarization techniques are in good agreement. At large Q^2 , however, the cross section data [2–5] disagree with the ratios G_E/G_M obtained using the polarization transfer method [6–9]. This systematic difference is a source of intense debate in both the theoretical and experimental nuclear physics communities.

Recently, theoretical attention has been paid to the set of radiative corrections [10, 11] that must be made to the cross section data in order to extract the form factor ratio. These corrections change the slope of the reduced cross section by as much as 30% for larger Q^2 . In contrast, radiative corrections to the polarization data are essentially negligible [12]. Until recently, only “standard” radiative corrections were taken into account. Based on the observed discrepancy in the data, new efforts have been made to include higher-order radiative mechanisms, such as two-photon exchange (TPEX) [13–19]. Several of these calculations have indicated that TPEX partially resolves the disagreement between the two data sets, but further investigation is needed. What is still lacking is a complete set of elastic ep scattering observables sensitive to the TPEX amplitudes, with sufficient precision to guide the development of a consistent theoretical framework for the interpretation of the discrepancy in terms of TPEX. This experiment is an effort to provide additional data.

When considering the exchange of two or more photons, the hadronic vertex function can generally be expressed, in terms of three independent and complex amplitudes, $\tilde{G}_{E,M} \equiv G_{E,M}(Q^2) + \delta\tilde{G}_{E,M}(Q^2, \epsilon)$ and \tilde{F}_3 which are functions of Q^2 and the kinematical parameter $\epsilon = (1 + 2(1 + \tau) \tan^2 \theta_e/2)^{-1}$, where $\tau \equiv Q^2/4M^2$, M

is the proton mass, and θ_e is the electron scattering angle. In the Born approximation, the first two amplitudes equal the real electric and magnetic Sachs form factors which depend only on Q^2 , and \tilde{F}_3 vanishes. The experimental observables used to extract G_{Ep} and G_{Mp} from cross section and polarization transfer measurements, assuming the validity of the Born approximation, are affected in different ways by TPEX, as shown in Eq.(1). The Rosenbluth method relies on measuring the ϵ dependence of the reduced cross section σ_r at fixed Q^2 to separate G_E^2 from G_M^2 , and becomes highly sensitive to additive TPEX effects at large Q^2 when $\epsilon G_E^2/\tau G_M^2$ becomes small. The transferred polarization to the recoil proton in $H(\vec{e}, e'\vec{p})$ has transverse (P_t) and longitudinal (P_ℓ) components with respect to the momentum transfer in the scattering plane [20, 21]. The ratio R defined in Eq.(1) equals $\mu_p G_E/G_M$ in the Born approximation, and is much less vulnerable to TPEX corrections. The TPEX corrections appear in σ_r , P_t , P_ℓ , and R as interference terms between the Sachs form factors and the real part of the TPEX amplitudes [22]:

$$\begin{aligned}
P_t &= -\frac{hP_e}{\sigma_r} \sqrt{\frac{2\epsilon(1-\epsilon)}{\tau}} \left[G_E G_M + G_M \Re(\delta\tilde{G}_E + \frac{\nu}{M^2} \tilde{F}_3) \right. \\
&\quad \left. + G_E \Re(\delta\tilde{G}_M) + \mathcal{O}(e^4) \right] \\
P_\ell &= \frac{hP_e}{\sigma_r} \sqrt{1-\epsilon^2} \left[G_M^2 + 2G_M \Re(\delta\tilde{G}_M + \frac{\nu}{M^2} \frac{\epsilon}{1+\epsilon} \tilde{F}_3) \right. \\
&\quad \left. + \mathcal{O}(e^4) \right] \\
\sigma_r &= G_M^2 + \frac{\epsilon}{\tau} G_E^2 + \frac{2\epsilon}{\tau} G_E \Re(\delta\tilde{G}_E + \frac{\nu}{M^2} \tilde{F}_3) \\
&\quad + 2G_M \Re(\delta\tilde{G}_M + \frac{\epsilon\nu}{M^2} \tilde{F}_3) + \mathcal{O}(e^4) \\
R &\equiv -\mu_p \sqrt{\frac{(1+\epsilon)\tau}{2\epsilon}} \frac{P_t}{P_\ell} = \mu_p \frac{G_E}{G_M} \Re \left[1 - \frac{\delta\tilde{G}_M}{G_M} + \frac{\delta\tilde{G}_E}{G_E} \right. \\
&\quad \left. + \frac{\nu\tilde{F}_3}{M^2} \left(\frac{1}{G_E} - \frac{2\epsilon}{1+\epsilon} \frac{1}{G_M} \right) \right] + \mathcal{O}(e^4) \quad (1)
\end{aligned}$$

where \Re stands for the real part, $h = \pm 1$ and P_e are the helicity and polarization of the electron beam, and $\nu = M \frac{E_e + E'_e}{2}$, with E_e, E'_e being the energy of the incident and scattered electron, respectively. In the Born approximation, these corrections vanish and the well known expressions for these observables [20, 21] are recovered. Other observables, such as the induced normal polarization component, and the target-normal and beam-normal single-spin asymmetries, depend only on the imaginary (absorptive) part of the TPEX amplitude. A direct

test of the TPEX effect is the comparison between e^+p and e^-p elastic scattering cross sections. Since the two-photon contributions (relative to the Born amplitudes) are of opposite sign, a few percent deviation from unity as a function of ϵ is predicted for the ratio $\sigma_{e^+}/\sigma_{e^-}$. Recent analyses of $e^\pm p$ cross sections are inconclusive due to large uncertainties in the data [23–25].

In this experiment, carried out at Jefferson Lab in Hall C, a longitudinally polarized electron beam (82-86% polarization) was scattered elastically off a 20 cm liquid hydrogen target at $Q^2 = 2.5 \text{ GeV}^2$. Electrons were detected by a 1744 channel lead-glass electromagnetic calorimeter (BigCal), which measured their coordinates and energy. Overlapping analog sums of up to 64 channels were used to form the BigCal trigger with a threshold of about half the elastic electron energy. Coincident protons were detected in the High Momentum Spectrometer (HMS) [26]. The HMS trigger was formed from a coincidence between a scintillator plane located behind the drift chambers and an additional paddle placed in front of the drift chambers. The polarization of scattered protons, after undergoing spin precession in the HMS magnets, was measured by the Focal Plane Polarimeter (FPP), which consists of an assembly of two 55 cm thick CH_2 analyzer blocks, each followed by a pair of drift chambers to track re-scattered protons with an angular resolution of approximately 1 mrad. Elastic event selection was performed offline in the same way as explained in [9], resulting in a very small inelastic contamination for all three kinematics; at $\epsilon = 0.15$, where it is the highest, the background fraction is 0.7%.

The scattered proton polarization was obtained from the angular distribution of protons scattered in the analyzer blocks of the FPP. The polar and azimuthal scattering angles (ϑ, φ) of single-track events in the FPP chambers were calculated relative to the incident track defined by the HMS drift chambers. The difference and the sum of the azimuthal angular distributions for positive and negative beam helicities give the physical (helicity-dependent) and instrumental or false (helicity-independent) asymmetries at the focal plane, respectively.

Since the proton polarization components are measured at the focal plane, knowledge of the spin transport matrix of the HMS is needed to obtain P_t and P_ℓ at the target. The differential-algebra based modeling program COSY [27] was used to calculate the spin-transport matrix elements for each event from a detailed layout of the HMS magnetic elements. The quantities $P_e A_y P_t$ and $P_e A_y P_\ell$ were extracted using the maximum-likelihood method described in [8, 9], with A_y the analyzing power of $\vec{p} + \text{CH}_2 \rightarrow \text{one charged particle} + X$ scattering. Their ratio gives P_t/P_ℓ independent of A_y and P_e .

As an example of the quality of the data, Fig.1 shows R and $A_y P_\ell$ as a function of the vertical (dx/dz) and horizontal (dy/dz) slopes of the scattered proton trajectory

relative to the HMS optical axis. Owing to the small acceptance of the HMS in both ϵ and Q^2 for all three kinematics, R and $A_y P_\ell$ are constant across the acceptance to a very good approximation. The absence of anomalous dependence of the extracted R and $A_y P_\ell$ on the reconstructed kinematics is thus an important test of the accuracy of the field description in the COSY calculations. In each panel of Fig. 1, the data are integrated over the full acceptance of all other variables. The horizontal line shows the one-parameter fit to the extracted data. In all panels, the χ^2 per degree of freedom is close to one, indicating the excellent quality of the precession calculation.

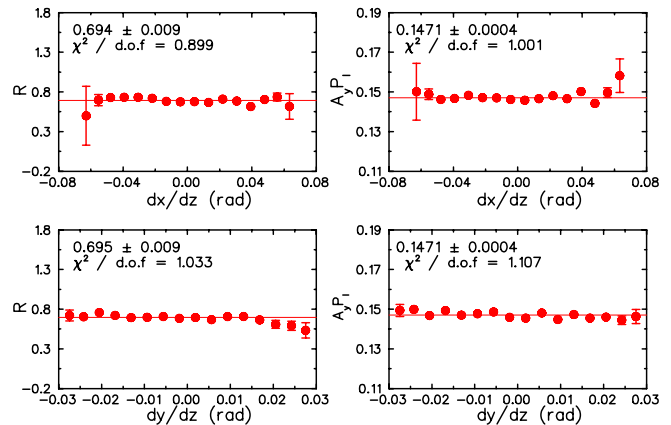


FIG. 1: R (left column) and $A_y P_\ell$ (right column) versus the dispersive dx/dz (vertical) and non-dispersive dy/dz (horizontal) slopes for the low-energy setting using the COSY model.

The main results of this experiment are given in Table I and shown in Fig. 2. Figure 2a displays R as a function of ϵ with selected theoretical estimates. The data do not show any evidence of an epsilon dependence of R at $Q^2 = 2.5 \text{ GeV}^2$. Both statistical and point-to-point systematic uncertainties (relative to the largest ϵ kinematic) are shown in the figure. The *total* systematic uncertainties in R are shown in Table I. For a given data point, the point-to-point systematics are obtained as the quadrature sum over the differences between each of the systematic contribution and the corresponding one for a reference kinematic. Because the dominant sources of systematic uncertainty described below affect R for all three kinematics in a strongly correlated fashion, the systematic uncertainty on the relative variation of R as a function of ϵ , characterized by the point-to-point uncertainties, is very small.

Another sensitive probe of two-photon effects is taking the ratio of the measured P_ℓ to P_ℓ^{Born} , where P_ℓ^{Born} is P_ℓ calculated in the Born approximation. In the limit $\epsilon \rightarrow 0$, angular momentum conservation requires $P_\ell \rightarrow 1$, independent of R (see Eq. 1); for our measurement at $\epsilon = .15$, P_ℓ varies by only 1.4% (relative) [28] for R be-

TABLE I: Kinematic table with the average quantities: the beam energy E_e , the momentum transfer squared Q^2 , the electron scattering angle θ_e , and the kinematical parameter ϵ . Both the ratio R and longitudinal polarization P_ℓ divided by Born approximation P_ℓ^{Born} are given with statistical (stat.), total systematic (tot.) and point-to-point (p.t.p.) uncertainties relative to the highest ϵ point for R and to the lowest ϵ kinematic for P_ℓ/P_ℓ^{Born} .

$\langle E_e \rangle$ (GeV)	$\langle Q^2 \rangle$ (GeV ²)	$\langle \theta_e \rangle$ (°)	ϵ	$R \pm stat. \pm p.t.p.$	tot.	$P_\ell/P_\ell^{Born} \pm stat. \pm p.t.p.$	tot.
1.87	2.493	104.0	0.152 $\pm_{0.030}^{0.025}$	0.696 $\pm 0.009 \pm 0.006$	0.013	—	—
2.84	2.490	44.6	0.635 $\pm_{0.017}^{0.013}$	0.688 $\pm 0.011 \pm 0.001$	0.009	1.007 ± 0.005	± 0.005
3.63	2.490	31.7	0.785 $\pm_{0.010}^{0.008}$	0.692 $\pm 0.011 \pm 0.000$	0.009	1.023 ± 0.006	± 0.005

tween 0 and 1. Therefore, the measured value of $hA_y P_\ell$ at $\epsilon = .15$ determines $\bar{A}_y = 0.15079 \pm 0.00038$ (specific to this polarimeter), corresponding to a relative uncertainty of 0.25%, included in the statistical error budget for P_ℓ/P_ℓ^{Born} . Applying the same phase space cuts at the focal plane results in A_y being the same for all three kinematics, at the 10^{-3} level. P_ℓ^{Born} was calculated from the beam energy, the proton momentum, and the fitted value of R from this experiment, with the errors in each quantity accounted for in the total systematic error in P_ℓ/P_ℓ^{Born} . In Fig. 2b, the ratio P_ℓ/P_ℓ^{Born} is plotted versus ϵ . The results show an enhancement at large epsilon of $2.3 \pm 0.6\%$ relative to the Born approximation.

The number of sources of systematic uncertainty is drastically reduced by the fact that the beam helicity and the polarimeter analyzing power cancel out exactly in the ratio of polarization components. Consequently, the spin precession uncertainty is the dominant contribution. Since the central proton momentum was fixed across the three kinematics, the spin transport matrix is identical, resulting in small point-to-point systematic uncertainties. The error $\Delta\phi_{bend} = \pm 0.5$ mrad in the non-dispersive bend angle, due to uncertainty in the HMS quadrupole positions, represents the largest contribution. The uncertainty of $\pm 0.1\%$ in the absolute determination of the proton momentum, which has a negligible effect on the precession uncertainty in P_t/P_ℓ , leads to a relative uncertainty in the kinematic factor $\sqrt{\tau(1+\epsilon)}/2\epsilon$ that is roughly 1/3 of the relative uncertainty in P_t/P_ℓ at the lowest ϵ , but negligible at higher ϵ . Errors in the dispersive bend angle, the beam energy, and the scattering angle in the FPP give smaller contributions. The inclusion of instrumental asymmetry terms obtained from Fourier analysis of the helicity-independent asymmetries in the likelihood function induces a negative correction to R ($|\Delta R| \leq 0.013$) and P_ℓ/P_ℓ^{Born} ($|\Delta P_\ell/P_\ell^{Born}| \leq 0.004$) for each ϵ value. A systematic uncertainty equal to half the false asymmetry correction was included in the total systematic uncertainty on R and P_ℓ/P_ℓ^{Born} . A 1% absolute systematic uncertainty (0.5% point to point) from the Möller measurements of the beam polarization was added to the error budget of P_ℓ/P_ℓ^{Born} . In order to minimize systematic differences in the spin transport calculation among the three kinematics, cuts were applied

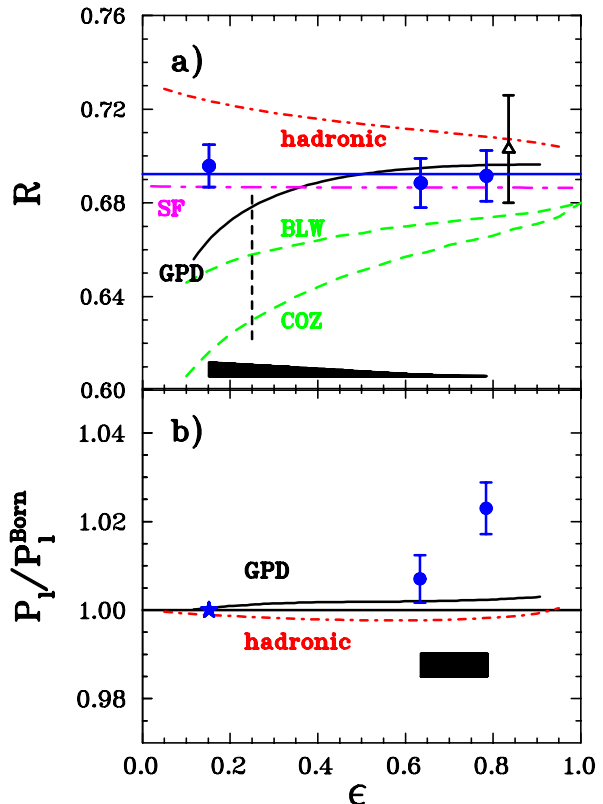


FIG. 2: a) R as a function of ϵ with statistical uncertainties, filled circles from this experiment and open triangle from [7]. The theoretical predictions are from: [14] (hadronic), [13] (GPD), [19] (COZ and BLW) and [17] (SF) offset for clarity by -0.006 with respect to the fit. The one parameter fit result is: $R = 0.6923 \pm 0.0058$. b) P_ℓ/P_ℓ^{Born} as a function of ϵ . The point-to-point systematic uncertainties, shown with a band in both panels, are relative to the largest ϵ kinematic in a) and relative to the smallest ϵ kinematic in b). The star indicates the ϵ value at which the analyzing power is determined.

to the focal plane trajectories of the data for the two larger ϵ points to match the smaller acceptance of the point at $\epsilon = 0.15$. The program MASCARAD [12] was used to compute “standard” radiative corrections to R . Small, positive corrections ΔR of 1.2×10^{-3} , 1.4×10^{-4} and 0.7×10^{-4} were found for $\epsilon = 0.15$, 0.63 , and 0.78 , respectively. The corrections to P_ℓ/P_ℓ^{Born} were found to

be even smaller. The results shown in Table I do not include these corrections.

The theoretical curves shown in Figure 2a make widely varying predictions for the epsilon dependence of R . The hadronic model of Blunden *et al.* [14], where all the proton intermediate states are taken into account via a complete calculation of the loop integral using 4-point Passarino-Veltman functions [29], shows a significant positive TPEX contribution at small ϵ . The inclusion of higher resonances makes almost no difference [15]. On the contrary, the partonic model of Afanasev *et al.* [13], where the TPEX takes place in a hard scattering of the electron by quarks which are embedded in the nucleon through the GPDs, predicts a negative TPEX contribution. A pQCD calculation of Kivel and Vanderhaeghen [19], which uses two different light front proton distribution amplitude parametrizations, one from Chernyak *et al.* (COZ) [30] and the other one from Braun *et al.* (BLW) [31], presents a behaviour similar to the partonic model. The limit of applicability of the GPD and pQCD models is shown by the vertical dashed line on the figure. The electron structure function (SF) based model developed by Bystritskiy *et al.* [17], which takes into account all high order radiative corrections in the leading logarithm approximation, does not predict any measurable ϵ dependence of R . The GPD, hadronic and pQCD models, while in good agreement with the available cross section data, predict a deviation of R at small ϵ due to modification in P_t ; not seen in the results presented here. Referring to Eq.(1), R is directly proportional to the Born value G_E/G_M , so all the theory predictions, which use a G_E/G_M value from [6–8], can be renormalized by an overall multiplicative factor. The enhancement seen in P_ℓ/P_ℓ^{Born} is not predicted by any models. The behavior of R at large ϵ implies the same deviation of P_t from its Born value as the one observed in P_ℓ/P_ℓ^{Born} .

The high precision data presented in this letter add significant constraints on possible solutions of Eq.(1) for the real part of the TPEX amplitudes [32]. In this experiment, no ϵ dependence was found in R , suggesting that the 2γ amplitudes are small or compensate each other in the ratio. The study of the non-linearity of the Rosenbluth plot, a precise measurement of the single spin asymmetries and the determination of the $\sigma_{e^+}/\sigma_{e^-}$ ratio are essential to fully understand, quantify and characterize the two-photon-exchange mechanism in electron proton scattering.

The GEp2 γ collaboration thanks the Hall C technical staff and the Jefferson Lab Accelerator Division for their outstanding support during the experiment. This work was supported in part by the U.S. Department of Energy, the U.S. National Science Foundation, the Italian Institute for Nuclear research, the French Commissariat à l’Energie Atomique (CEA), the Centre National de la Recherche Scientifique (CNRS), and the Natural Sciences and Engineering Research Council of Canada. This work

is supported by DOE contract DE-AC05-06OR23177, under which Jefferson Science Associates, LLC, operates the Thomas Jefferson National Accelerator Facility.

* Corresponding author: mezzianem@jlab.org

† Deceased.

- [1] M. N. Rosenbluth, Phys. Rev. **79**, 615 (1950).
- [2] C. Perdrisat, V. Punjabi, and M. Vanderhaeghen, Prog. Part. Nucl. Phys. **59**, 694 (2007).
- [3] L. Andivahis *et al.*, Phys. Rev. D **50**, 5491 (1994).
- [4] M. E. Christy *et al.*, Phys. Rev. C **70**, 015206 (2004).
- [5] I. A. Qattan *et al.*, Phys. Rev. Lett. **94**, 142301 (2005).
- [6] M. K. Jones *et al.*, Phys. Rev. Lett. **84**, 1398 (2000).
- [7] V. Punjabi *et al.*, Phys. Rev. C **71**, 055202 (2005).
- [8] O. Gayou *et al.*, Phys. Rev. Lett. **88**, 092301 (2002).
- [9] A. J. R. Puckett *et al.*, Phys. Rev. Lett. **104**, 242301 (2010).
- [10] L. M. Mo and Y. S. Tsai, Phys. Rev. **41**, 205 (1969).
- [11] R. C. Walker *et al.*, Phys. Rev. D **49**, 5671 (1994).
- [12] A. Afanasev, I. Akushevich, and N. Merenkov, Phys. Rev. D **64**, 113009 (2001).
- [13] A. V. Afanasev, S. J. Brodsky, C. E. Carlson, Y.-C. Chen, and M. Vanderhaeghen, Phys. Rev. D **72**, 013008 (2005).
- [14] P. G. Blunden, W. Melnitchouk, and J. A. Tjon, Phys. Rev. C **72**, 034612 (2005).
- [15] S. Kondratyuk, P. G. Blunden, W. Melnitchouk, and J. A. Tjon, Phys. Rev. Lett. **95**, 172503 (2005).
- [16] J. Arrington, Phys. Rev. C **71**, 015202 (2005).
- [17] Y. M. Bystritskiy, E. A. Kuraev, and E. Tomasi-Gustafsson, Phys. Rev. C **75**, 015207 (2007).
- [18] C. E. Carlson and M. Vanderhaeghen, Ann. Rev. Nucl. Part. Sci. **57**, 171 (2007), hep-ph/0701272.
- [19] N. Kivel and M. Vanderhaeghen, Phys. Rev. Lett. **103**, 092004 (2009).
- [20] A. I. Akhiezer and M. P. Rekalov, Sov. J. Part. Nucl. **3**, 277 (1974).
- [21] R. G. Arnold, C. E. Carlson, and F. Gross, Phys. Rev. C **23**, 363 (1981).
- [22] P. A. M. Guichon and M. Vanderhaeghen, Phys. Rev. Lett. **91**, 142303 (2003).
- [23] J. Arrington, Phys. Rev. C **69**, 032201 (2004).
- [24] E. Tomasi-Gustafsson, M. Osipenko, E. A. Kuraev, Y. Bystritskiy, and V. V. Bytev, ARXIV:0909.4736 (2009).
- [25] W. M. Alberico, S. M. Bilenky, C. Giunti, and K. M. Graczyk, J. Phys. G **36**, 115009 (2009).
- [26] H. P. Blok *et al.*, Phys. Rev. C **78**, 045202 (2008).
- [27] K. Makino and M. Berz, Nucl. Instrum. Methods A **427**, 338 (1999).
- [28] L. Pentchev, AIP Conference Proceedings **1056**, 357 (2008).
- [29] G. Passarino and M. Veltman, Nucl. Phys. B **160**, 151 (1979).
- [30] V. L. Chernyak, A. A. Ogloblin, and I. Zhitnitsky, Z. Phys. C **42**, 569 (1989).
- [31] V. M. Braun, A. Lenz, and M. Wittmann, Phys. Rev. D **73**, 094019 (2006).
- [32] J. Guttman, N. Kivel, M. Mezziane, and M. Vanderhaeghen, ARXIV:1012.0564 (2010).